THE IIOAB JOURNAL

VOLUME 11 : NO 2 : AUGUST 2020 : ISSN 0976-3104

SUPPLEMENT ISSUE

Institute of Integrative Omics and Applied Biotechnology Journal

Dear Esteemed Readers, Authors, and Colleagues,

I hope this letter finds you in good health and high spirits. It is my distinct pleasure to address you as the Editor-in-Chief of Integrative Omics and Applied Biotechnology (IIOAB) Journal, a multidisciplinary scientific journal that has always placed a profound emphasis on nurturing the involvement of young scientists and championing the significance of an interdisciplinary approach.

At Integrative Omics and Applied Biotechnology (IIOAB) Journal, we firmly believe in the transformative power of science and innovation, and we recognize that it is the vigor and enthusiasm of young minds that often drive the most groundbreaking discoveries. We actively encourage students, early-career researchers, and scientists to submit their work and engage in meaningful discourse within the pages of our journal. We take pride in providing a platform for these emerging researchers to share their novel ideas and findings with the broader scientific community.

In today's rapidly evolving scientific landscape, it is increasingly evident that the challenges we face require a collaborative and interdisciplinary approach. The most complex problems demand a diverse set of perspectives and expertise. Integrative Omics and Applied Biotechnology (IIOAB) Journal has consistently promoted and celebrated this multidisciplinary ethos. We believe that by crossing traditional disciplinary boundaries, we can unlock new avenues for discovery, innovation, and progress. This philosophy has been at the heart of our journal's mission, and we remain dedicated to publishing research that exemplifies the power of interdisciplinary collaboration.

Our journal continues to serve as a hub for knowledge exchange, providing a platform for researchers from various fields to come together and share their insights, experiences, and research outcomes. The collaborative spirit within our community is truly inspiring, and I am immensely proud of the role that IIOAB journal plays in fostering such partnerships.

As we move forward, I encourage each and every one of you to continue supporting our mission. Whether you are a seasoned researcher, a young scientist embarking on your career, or a reader with a thirst for knowledge, your involvement in our journal is invaluable. By working together and embracing interdisciplinary perspectives, we can address the most pressing challenges facing humanity, from climate change and public health to technological advancements and social issues.

I would like to extend my gratitude to our authors, reviewers, editorial board members, and readers for their unwavering support. Your dedication is what makes IIOAB Journal the thriving scientific community it is today. Together, we will continue to explore the frontiers of knowledge and pioneer new approaches to solving the world's most complex problems.

Thank you for being a part of our journey, and for your commitment to advancing science through the pages of IIOAB Journal.

Yours sincerely,

Vasco Azevedo

Vasco Azevedo, Editor-in-Chief
Integrative Omics and Applied Biotechnology
(IIOAB) Journal

ISSN: 0976-3104
ISSUE: Science and Technology

ARTICLE

FATIGUE STRENGTH OF ALUMINIUM ALLOY STRUCTURES

Korgin Andrey Valentinovich*, Romanets Vladimir Anatolyevich

Moscow State University of Civil Engineering (MGSU), Yaroslavskoye Shosse, 26, Moscow, 129337, RUSSIA

ABSTRACT

This article proposes fatigue strength calculation method for building structures made of aluminium alloys, which has not been included in codes and standards of the Russian Federation until now. For this purpose, conducted complex laboratory tests were made on three aluminium alloys which might be potentially used in building structures production: 1915T, AD35T1, 1565chM. As the result of the tests. stress-strain and fatigue properties of these alloys were obtained. The proposed method is based on home-grown developments for steel building structures fatigue strength calculation and foreign data on aluminium structures fatigue strength calculation. Accuracy of the method has been checked during numerical simulation as well as static and fatigue tests of full-size walking bridge made of 1915T alloy. Deviations from the results of calculation performed using this method were equal to no more than 5-15%.

KEY WORDS
building structure, bridge, test of specimens, calculation method, stress

INTRODUCTION

Modern trends in industry and building development are based on increasingly wide application of innovative technologies and materials. Aluminium is certainly at the top of the list of such materials due to its wide application in many industries – aviation, electrical engineering, automotive engineering, transport, building structures, etc [1].

Application of aluminium for production of different structures gives some important advantages as compared to conventional materials [2]:

- low specific gravity as compared to other metals;
- high specific strength exceeding specific strength of steel and concrete;
- no tendency to brittle fracture in case of temperature decrease;
- increased seismic stability of structures due to lower weight;
- high corrosion resistance of some alloys;
- manufacturability of structural members having different shapes;
- easy transportation and mounting of large-sized fragments.

At the same time, aluminium alloy structures have some disadvantages:

- increased deformability due to decreased modulus of elasticity;
- relatively low resistance to fatigue fracture;
- risk of galvanic corrosion in the points of contact with other materials.

Received: 6 Feb 2020
Accepted: 7 Apr 2020
Published: 10 Apr 2020

It should be noted that disadvantages listed above can be minimized or even eliminated in the course of development due to special design solutions and measures.

Until the present time, fatigue strength calculation method for aluminium alloys has not been included in the regulatory documents of the Russian Federation for building structures design [3]. It was mainly due to the lack of scientific research on fatigue behaviour of aluminium alloys in building structures.

The main objectives of this work are experimental studies of the fatigue properties of aluminum alloys and the development of fatigue strength calculation methods for building structures made of these alloys on the basis of the obtained results.

FATIGUE STRENGTH CALCULATION METHOD

As aluminium alloys are widely used in structures being subjected to time-varying cyclical influences such as more and more widespread motor-road and walking bridges, the necessity to provide endurance of such alloys throughout their specified service life becomes more and more important. Service life of such structures may account for several decades and the number of load cycles during their service life may be up to $10^6 \div 10^8$ and more [4].

***Corresponding Author**
Email:
korguine@mgsu.ru

Basic cyclic load parameters are minimum and maximum cycle stresses σ_{max}, σ_{min}. Cycle amplitude σ_a and mean cycle stress σ_m determined on the base thereof as well as stress ratio r are interrelated by the following equations:

$$\sigma_a = \frac{\sigma_{max} - \sigma_{min}}{2}, \ \sigma_m = \frac{\sigma_{max} + \sigma_{min}}{2} \quad (1)$$

$$r = \frac{\sigma_{min}}{\sigma_{max}}, \quad (2)$$

Metals (fatigue) strength is characterized by fatigue strength curve obtained as the result of fatigue tests on the series of smooth specimens at different levels of cyclic stresses (σ_a-N curve – [Fig. 1]). This curve presented in coordinates logσ_a – log$N$ (σ_a – cycle amplitude, N – number of load cycles) has a shape of broken curve consisting of straight-line portions.

The main material fatigue characteristic is fatigue strength σ_r, which is determined by fatigue curve and represents the maximum stress, below which there is no fatigue fracture (fatigue crack formation) in material, or material is able to withstand the specified number of load cycles.

Fatigue curve for most steels has two intrinsic portions [Fig. 1a]: slopped portion with slope angle defined by parameter m_1, and plateau conforming to fatigue strength value achieved at approximately10^7 load cycles [5, 6].

In contrast to steels, this curve for aluminium alloys has more complex shape including three portions [Fig. 1b], slopped portions have different slope angles expressed by parameters m_1, $m_2 \cong m_1+2$, and plateau is achieved later than for steels, at approximately 10^8 load cycles [4, 7].

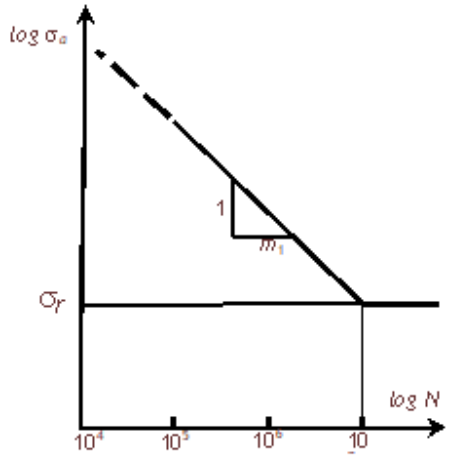

Fig. 1a

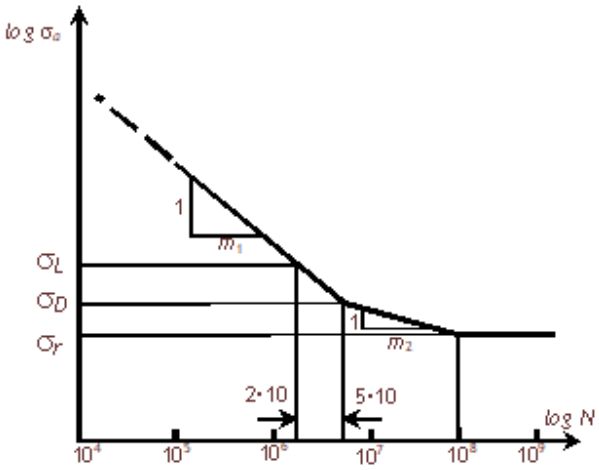

Fig. 1b

σ_r is the fatigue strength at specified load cycle (for symmetric cycle $\sigma_r = \sigma_{-1}$: for steels at 10^7 cycles, for aluminium alloys at $2{\cdot}10^6$ cycles);
σ_D is the fatigue strength for aluminium alloys at $5{\cdot}10^6$ cycles;
σ_L is the damage threshold for aluminium alloys at (10^8 cycles).

Factors influencing fatigue strength value

Stress concentration

Fatigue fracture accompanied by fatigue cracks formation usually occurs in stress concentration areas of the most loaded structural members due to their shape and interconnection methods.

Actual values of cycle amplitude σ'_a and mean cycle stress σ'_m in expected fatigue fracture area are called effective stresses. They are determined by multiplication of nominal values of cycle amplitude σ'_a and mean cycle stress σ'_m by theoretical stress concentration factor K_σ:

$$\sigma'_a = \sigma_a K_\sigma. \quad (3)$$

Nominal stresses σ_a, σ_m in the said zones are determined by static structural calculation without regard to stress concentration effect.

IIOAB JOURNAL
ISSN: 0976-3104

Structural members manufacturing quality

Structural members manufacturing quality is taken into account in fatigue calculations using manufacturing method dependent safety margin γ_{Mf}, depending on processing method used during fabrication of structural members made of aluminium alloys [Table 1] [8].

Table 1: Method used in fabrication

Manufacturing method	γ_{Mf}
Rolled and molded sections	1,0
Automatic cutting from metal sheet with edges milling and holes broaching	1,1
Automated cutting from metal sheet without edges and holes processing	1,2–1,3
Cold-formed section from metal sheet	1,5

Structural members interconnection method

Structural members interconnection method is taken into account in fatigue calculations using interconnection method dependent safety margin γ_{Sf}, depending on the method used for structural members interconnection in structural units [Table 2] [8].

Table 2: Method used for interconnection of structural units

Interconnection method	γ_{Sf}
Friction stir welding	1,1
Semiautomatic argon arc inert-gas shielded welding	1,3
Manual argon arc welding	1,5
Interconnection using high-strength bolts with tightening force control	1,2

Rolled thickness

Thickness-dependent safety margin γ_{TF}=1.05 is introduced when manufacturing structural members from aluminium alloys with rolled thickness above 50 mm and γ_{TF}=1.0 for lower thickness [8].

Stress ratio r

Stress ratio *r* has great impact on fatigue strength of structural members [6, 7].

Fatigue curves for random aluminium alloy tested with different values of stress ratio *r* are shown in [Fig. 2a].

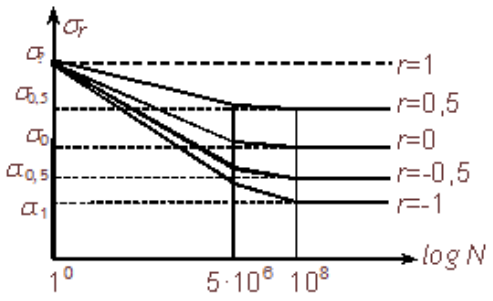

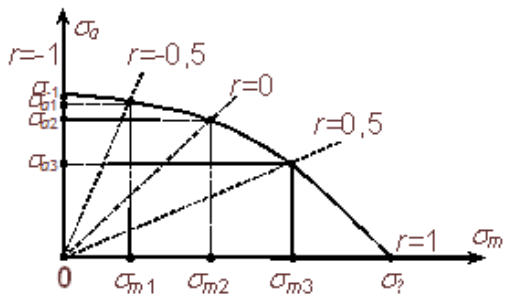

Fig. 2a **Fig. 2b**

Zero point on horizontal axis conforms to static destructive test which gives the value of ultimate strength $\sigma_в$ on vertical axis (stress ratio *r*=1).

Next curves give fatigue strength σ_r values in the range of $-1 < r \leq 1$; the lowest value of fatigue strength σ_{-1} occurs with symmetric cycle (*r*=–1), which is most dangerous in the context of fatigue fracture point.

Fatigue strength values obtained at different values of stress ratio *r* in coordinates σ_a, σ_m (cycle amplitude and mean cycle stress) form so called limiting amplitude diagram [Fig. 2b], conforming to the basic fatigue strength condition, at which maximum cycle stress shall not exceed corresponding fatigue strength σ_r:

$$\sigma_{max} = \sigma_a + \sigma_m \leq \sigma_r \quad (3)$$

Basically, limiting amplitude diagram for specific alloy represents a complex strength characteristic of this alloy providing fatigue strength conditions in the range of stress ratio values -1≤ *r* ≤ 1.

Since it is impossible to perform a large number of fatigue tests, in practice approximated limiting amplitude diagrams [Fig. 3] built based on 2 or 3 standard tests are used [6, 7].

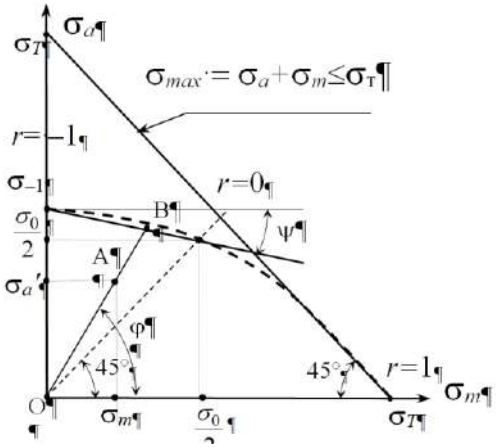

Fig. 3a

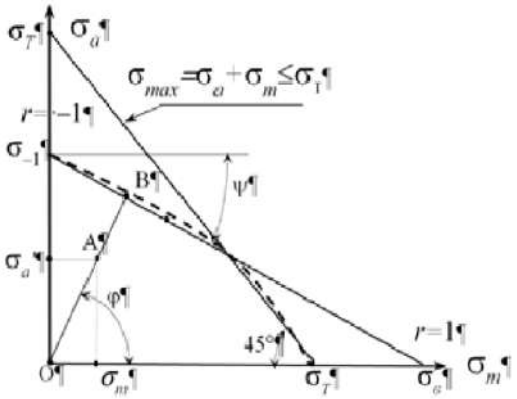

Fig. 3b

Approximated limiting amplitude diagram by Serensen – Kinasoshvili [8] [Fig. 3a] is built based on the results of two fatigue tests with stress ratios *r*=-1 (symmetric cycle) and *r*=0 (pulsed cycle) and static test used to determine yield strength σ_T (conventional yield strength $\sigma_{0,2}$ for alloys without yield plateau) which serves, together with fatigue strength condition (3), as static strength condition observance criterion:

$$\sigma_{max} = \sigma_a + \sigma_m \leq \sigma_T \quad (4)$$

Approximated limiting amplitude diagram by Goodman [Fig. 3b] [7, 9] is built based on the results of fatigue test with stress ratio *r*=-1 (symmetric cycle) and static test used to determine yield strength σ_T and ultimate strength $\sigma_в$ necessary for diagram construction. When using this diagram, error grows in its right portion together with the growth of stress ratio *r* positive values.

Effective values of cycle amplitude σ_a' and mean cycle stress σ_m at the given stress ratio *r* are shown on the diagram as a working point *A*.

Therefore, the main parameter expressed graphically using approximated limiting amplitude diagram is the actual fatigue fracture dependent safety margin Z_σ:

$$Z_\sigma = \frac{OB}{OA} \quad (5)$$

Fatigue strength calculation parameters, which are also obtained when building approximated limiting amplitude diagrams, are slope ratio ψ_σ:

for Serensen – Kinasoshvili diagram:

$$\psi_\sigma = \frac{2\,\sigma_{-1} - \sigma_0}{\sigma_0}, \quad (8)$$

for Goodman diagram:

$$\psi_\sigma = \frac{\sigma_{-1}}{\sigma_B}, \quad (9)$$

IIOAB JOURNAL
ISSN: 0976-3104

and asymmetric cycle slope ratio:

$$\varphi_\sigma = \frac{1-r}{1+r}, \tag{10}$$

where r is the stress ratio (1);
σ_{-1}, σ_0 are the fatigue strength at $2{\cdot}10^6$ load cycles with constant amplitude for symmetric (r=–1) and pulsed (r=0) cycles;
$\sigma_в$ is the ultimate strength.

In general, the value of actual fatigue strength dependent safety margin Z_σ for specific asymmetric load cycle is defined by geometric similarity analysis of approximated limiting amplitude diagram components [6, 8] and determined using the following equation:

$$Z_\sigma = \frac{\sigma_{-1}}{\sigma'_a + \sigma_m \psi_\sigma} = \frac{\sigma_{-1}}{\sigma_a K_\sigma + \sigma_m \psi_\sigma} = \frac{\sigma_{-1}}{\sigma_a (K_\sigma + \frac{\psi_\sigma}{\varphi_\sigma})}, \tag{11}$$

where σ_a, σ_a', σ_m are the nominal and effective values of cycle amplitude and mean cycle stress at asymmetric cycle with specified stress ratio r;
K_σ is the theoretical stress concentration factor.

In case of negative values of mean stress $\sigma_m < 0$ in the equation (11), its absolute value $|\sigma_m|$ is used.

In practice, stress concentration is usually taken into account by combination of structural members in groups, for which the nominal value of maximum acceptable cycle amplitude $\sigma_{a0,5}$ is set, that provides structural member fatigue strength at $2{\cdot}10^6$ load cycles depending on connection point types when testing with stress ratio r=0,5 [4, 8, 10].

Maximum acceptable value of nominal amplitude σ_{a-1} (r=-1) of symmetric cycle for specific group of members is defined by the following equation for the purpose of the use of that components group for calculation with asymmetric stress cycle type:

$$\sigma_{a-1} = \sigma_{a0,5}\left(1 + \frac{\psi_\sigma}{\varphi_\sigma}\right) = \sigma_{a0,5}(1 + 3\psi_\sigma). \tag{12}$$

Then the actual fatigue strength dependent safety margin Z_σ for structural member groups at specified stress ratio r value is defined by the equation:

$$Z_\sigma = \frac{\sigma_{a-1}}{\sigma_{ar}\,(1+\frac{\psi_\sigma}{\varphi_\sigma})}, \tag{13}$$

where σ_{ar} is the nominal cycle amplitude value at specified stress ratio r;
φ_σ is the limiting amplitude diagram slope ratio at specified r value.

FATIGUE STRENGTH CALCULATION FOR STRUCTURES MADE OF ALUMINIUM ALLOYS

Basic conditions of fatigue strength assurance

The final goal of structure fatigue strength calculation is to avoid fatigue cracks formation in load-bearing structural members throughout their specified service life.

The mean standard number of cycles during specified service life, with the exposure of aluminium alloy structures to which shall not lead to fatigue cracks formation, is customary equal to $2{\cdot}10^6$ cycles [8] unless otherwise specified.

Method providing absence of damages throughout specified service life

The principle of method is based on evaluation of damage occurrence during specified service life of the structure using the lower fatigue strength evaluation and the upper fatigue load evaluation which provides service life calculation for safety margin [4, 8] determination.

For this purpose, load history analysis is performed, which consists in generation of stress spectrum in potential cracking areas. This information based on damage rate calculation is used to evaluate design safe service life T_S, which is then compared with specified service life T_L:

$$T_S = \frac{T_L}{D_L}. \quad (14)$$

Total damage rate D_L for the totality of cycles is calculated based on Miner damage accumulation as a sum of their damage rate shares using the following formula:

$$D_L = \sum \frac{n_i}{N_i} \quad (15)$$

and shall satisfy the condition:

$$D_L \le D_{\lim} \le 1 \quad (16)$$

where $D_{\lim}$ is the damage rate limit value generally taken to be equal to 1;
N_i is the durability conforming to loading by i-type cycles in quantity of n_i.

Fatigue load

Fatigue load is determined by analysis of all variable stress sources in a structure, namely:

- temporary live loads;
- loads caused by wind and seismic impacts;
- dynamic response to resonance effects and movement in constrained conditions;
- temperature variations.

Design values of fatigue load are determined based on analysis of specified load spectrum and cycle count which define certain cyclic load value range and number of repetitions of each range throughout the structure service life.

Variable amplitude fatigue load stress spectrum, for example, is defined by "pool" method [4] consisting in determination of the sequence of cycles with decreasing stress amplitude σ_{ai} [Fig. 4].

If the values of fatigue load F_{Ek} obtained according to the above conditions are not sufficiently reliable, safety margin γ_{Ff} is applied to load F_{Ek} to determine design load F_{Ed}:

$$F_{Ed} = F_{Ek}\,\gamma_{Ff} \quad (17)$$

where γ_{Ff} is the safety margin for fatigue loads [Table 3].

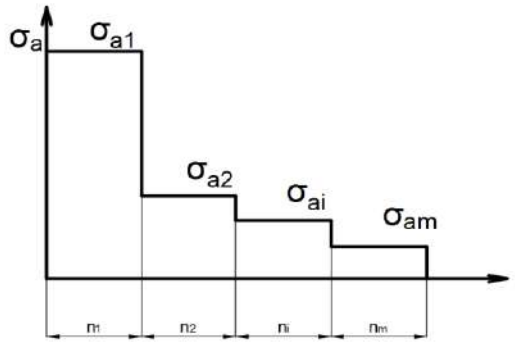

Fig. 4: Design base spectrum of effective load stress amplitudes

Table 3: The safety margin for fatigue loads

Number of standard deviations from the mean predictive load value K_F	γ_{Ff} at the given number of standard deviations from the mean predictive load cycles number	
	$K_N = 0$	$K_N = 2$
0	1.5	1.4
1	1.3	1.2
2	1.1	1.0

Stress state analysis

Analysis of structures stress state due to fatigue impacts is performed using elastic approach where maximum and minimum values of stresses caused by the given impact are determined taking account of possible dynamic effects.

Design values of effective stresses are obtained by:
– multiplication of nominal stresses by corresponding theoretical elastic stress concentration factors K_σ for linear-elastic material depending on cracking location and stress field type;
– finite element simulation of stress-strain behavior of possible cracking areas using detailed subdivision of these areas by finite elements of corresponding types.

Nominal cycle amplitude and mean cycle stress values according to equations (1-2) are adopted as design values used for fatigue strength evaluation with element clusters.

Fatigue strength calculation

Fatigue strength calculation consists in determination of structure damage rate shares due to the impact of each separate stress range from specified load spectrum [Fig. 4], which collectively provide the basic fatigue strength condition according to the equation (16).

For this purpose, durability values N_i are determined for all stress ranges from specified load spectrum conforming to the limit damage rate D_{lim}=1 due to the impact of each separate range. Total value of damage rate shares from each range is determined based on the equation (15).

Durability (design number of cycles to fracture) N_i for specific stress cycle range is defined using fatigue strength curve [Fig. 1b] [8]. N_i value within $5{\cdot}10^4 \div 5{\cdot}10^6$ cycles is determined using the formula:

$$N_i = N_{C1} \cdot \left(\frac{Z_\sigma}{[Z]}\right)^{m_1}, \tag{18}$$

N_i value within $5{\cdot}10^6 \div 5{\cdot}10^8$ cycles is determined using the formula:

$$N_i = N_{C2} \cdot \left(\frac{Z_\sigma}{[Z]}\right)^{m_2} \cdot C^{\frac{m_2}{m_1}}. \tag{19}$$

where $N_{C1}=2{\cdot}10^6$, $N_{C2}=5{\cdot}10^6$ (cycles);
$C=N_{C1}/N_{C2}=0{,}4$;
Z_σ is the actual fatigue strength dependent safety margin for the given cycle type determined by equations (11, 13);
$[Z]$ is the allowable fatigue strength dependent safety margin (20);
m_1, $m_2 \cong m_1+2$ are the fatigue strength curve portions slope parameters.

Values of allowable fatigue strength-dependent safety margin are determined taking account of structural members manufacturing quality, method of their interconnection in structural units and rolled thickness based on the equation:

$$[Z] = \gamma_{Mf} \cdot \gamma_{Sf} \cdot \gamma_{Tf}, \tag{20}$$

where γ_{Mf} is the structures manufacturing quality-dependent safety margin [Table 1];
γ_{Sf} is the interconnection method-dependent safety margin [Table 2];
γ_{Tf} is the rolled thickness-dependent safety margin (point 4).

If fatigue strength condition (16) is not met, it is necessary to change structural components cross section dimensions and repeat calculation until this condition is met.

RESULTS

Determination of physicomechanical characteristics of aluminum alloys

In order to validate the possibility of application of the above-mentioned fatigue strength calculation method for aluminium alloy structures, conducted static and fatigue laboratory tests on specimens were made of three aluminium alloys which might be potentially used in building structures production: 1915T, AD35T1, 1565chM [Fig. 5-6] [11].

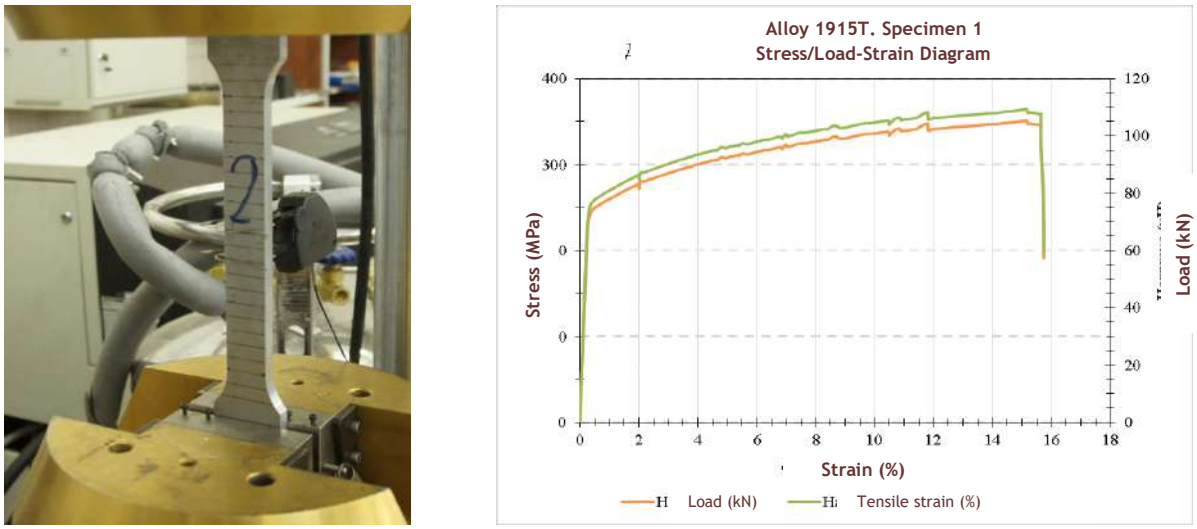

Fig. 5: View and results of static tests on specimens made of 1915T alloy

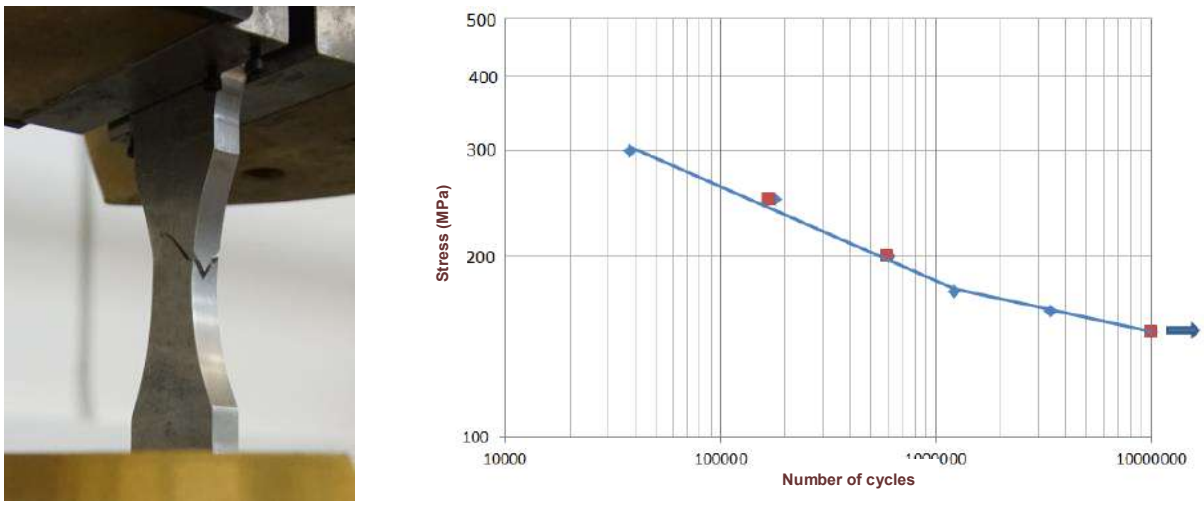

Fig. 6: View and results of fatigue tests on specimens made of 1915T aluminium alloy

During laboratory tests strength and fatigue properties of these alloys were determined. Basic properties are given in [Table 4].

Table 4

Parameter	Fatigue strength σ_{-1}, σ_0, yield strength σ_T, ultimate strength σ_B, MPa for alloys		
	1915T	AD35T1	1565chM
σ_{-1}	100	65	55

σ_0	150	105	90
σ_T	240	205	180
σ_B	360	320	270

Experimental validation of fatigue strength calculation method

Reliability of presented fatigue strength calculation method for structures made of aluminium alloys has been validated during the tests on structural members and actual walking bridge made of 1915T alloy [Fig. 7] [12].

Identification of the most stressed zones of bridge structures was carried out at the initial stage using finite element modeling, then the bridge was subjected to static loading, the results of which confirmed the conclusions of numerical modeling – the most stressed zones were the areas of the second struts from the edge of the bridge to the lower belts of the bridge load-bearing trusses.

The tests conducted had validated calculation method reliability. Discrepancies between experimental and theoretical data by the number of load cycles to fatigue cracking in the most stressed areas of the bridge were within 5-15%.

Fig. 7: View of the test on walking bridge made of 1915T aluminium alloy

CONCLUSION

The possibility of using the proposed calculation method of the fatigue strength of structures made of other aluminum alloys is determined, first of all, by the presence of their fatigue characteristics (fatigue strength for symmetric and pulsating cycles - σ_{-1}, σ_0). It should be borne in mind that the characteristics of the particular alloy depending on the conditions of its manufacture may differ significantly. For this reason, in the absence of these characteristics, it is necessary to conduct appropriate laboratory tests of samples and by full-scale tests of structures and their fragments made of this alloy. The advantage of the proposed method is in the use of two basic fatigue characteristics: fatigue strength for symmetric and pulsating cycles. This produces more reliable results compared to the main existing method [4] which uses only one value – fatigue strength at a given stress ratio.

CONFLICT OF INTEREST
None

ACKNOWLEDGEMENTS
None

FINANCIAL DISCLOSURE
None

REFERENCES

[1] Mikhailov GG, Bobrovnikov AP, Krasnenkova LV. [1983] Constructions of aluminum alloys. Metallurgy, Moscow.

[2] Hatch DE. [1989] Aluminium: properties and physical metallurgy. Metallurgy, Moscow.

[3] Code specification 128.13330.2016. Construction Standards and Regulations 2.03.06-85 "Aluminum structures".

[4] EN 1999-1-3:2007/A1-2011, Eurocode 9: Design of aluminium structures - Part 1-3: Structures susceptible to fatigue.
[5] Munze VH. [1968] Fatigue strength of welded steel structures. Mechanical Engineering, Moscow.
[6] Korgin AV. [2011] Strengths of materials with examples of task solutions in Microsoft Excel system, educational guidance. Infra-M, Moscow.
[7] Khazhinsky GM. [2016] Fundamentals of calculations for fatigue and long-term strength. Lenand, Moscow.
[8] Code specification 443.1325800.2019. Bridges with aluminium alloy structures. Design rules.
[9] Hwa P. [2001] Fatigue behaviour of 6061 aluminium alloy and its composite. Dublin City University.
[10] Code specification 16.13330.2011. Steel structures. Revised edition Construction Standards and Regulations II-23-81* with Amendment No. 1.
[11] Korgin AV, Odessky PD, Ermakov VA, Zeyd-Kilani LZ, Romanets VA, Koroleva EA. [2019] Strength of bridge engineering aluminium alloys. Strain and material damage, 8:10-19.
[12] Korgin A, Romanets V, Ermakov V, Zeyd-Kilani L. [2018] Experimental and analytical study of an aluminium alloy bridge made of 1915T. MATEC Web of Conferences, 251:04005.

ISSN: 0976-3104
ISSUE: Science and Technology

ARTICLE

INVESTIGATION ON THE STRENGTH BEHAVIORS OF RED MUD BASED PCM MORTAR

Gift Pon Lazarus D*, Sunita Bansal

Department of Civil Engineering, FET, MRIIRS, Faridabad, INDIA

ABSTRACT

In the housing sector, a large quantity of energy is expended on thermal comfort which increases the energy consumption and drives up demand, thus contributing to greenhouse gas emissions. The development of smart buildings and energy-efficient construction materials can reduce energy consumption and subsequent GHG emissions. The mortar used in building envelope can be customized to contain heat storage materials for moderating indoor temperature. The inert mortar composition of Phase Change Materials (PCMs) allows the absorption of heat during thermal weather and release of heat during cold weather due to phase transition from solid to liquid and liquid to solid. In this study, expanded graphite (EG) is used to encapsulate PCM to produce red mud based PCM mortar. Locally available red-mud, quartz sand, sodium silicate and sodium hydroxide mixture was used to produce a red-mud based PCM mortar. The variation in structural properties with different ratios of red mud and quartz sand was investigated to achieve the optimum ratio. The selection and application of the optimum mix in the outer walls of the building can thus be made on grounds of porosity, thermal conductivity and strength parameters.

KEY WORDS
Red-mud, Phase change material (PCM), Energy Efficient Buildings

Received: 17 Mar 2020
Accepted: 7 May 2020
Published: 20 May 2020

***Corresponding Author**
Email:
lazarusd.fet@mriu.edu.in
Tel.: +91-7358509997

INTRODUCTION

The building sector provides residential, commercial and other benefits to the community, however its contributions towards, the greatest global challenge and an indispensable requirement for sustainable development in the building sector is the reduction of greenhouse gas emissions and energy consumption and environmental degradation. In this regards, it is necessary the development and promotion of efficient, affordable, and high impact technologies, systems, and practices. The energy consumed for Heating, ventilating and air conditioning (HVAC) systems account for 60% of total energy in buildings. Phase Change Materials (PCM) integrated as building envelope materials to develop the performance of heating, ventilation and air-conditioning (HVAC) systems has been implemented as an energy efficiency measure [1]. To build Indian cities smart and sustainable, the energy consumption of building sector need to be reduced (Ministry of Urban Development, Government of India, 2015). The air-conditioning and lighting consumption can be reduced by integrating climate responsive techniques need to consider in the design [2].

The per capita energy usage defines the standards of living and economy of a country, thus, countries are focused on increasing their energy production capacity. Sun is a prime source of energy and utilization of this solar energy for building energy conservation can be a changing point in the energy storage potential of buildings. One of the techniques improving the thermal energy storage effective aspects of a building would be to adding the thermal mass of the building components by incorporating phase change materials (PCMs) within the building envelopes it helps to decreasing the temperature fluctuation and peak temperature within [3].

The working principle of the PCM is that it saving energy when liquefy and releases the energy when solidifies. The melting of the PCM happens during the daytime when the temperature due to the solar radiation is higher than the melting temperature of the PCM. Similarly, during the night solidification of the PCM happens, when the outside heat is lower than the melting temperature of the PCM. Hence, when PCM is incorporated into the building envelopes the heat storage ability of the building improves and substantially improves the indoor thermal behavior [4].

Due to the thermal features of phase change materials(PCMs), they have identified PCM integrated methods into common building envelope material, such as motor, concrete, wall, floor, ceiling and roofing tiles, boards, slate, bricks and interlocking bricks, paints, coatings and slabs are possible for thermal energy efficiency in buildings [5].

Phase Change Materials (PCMs) considered ‘‘latent’’ heat storage materials having a massive amount of heat energy stored during its phase change stage process. The thermal energy is required to change the phase of a substance is called as latent heat. There are two types of PCMs, organic and inorganic PCMs utilizing for building coated applications. Organic paraffin wax as one of the phase change material has capacity of heat absorbed or released when the paraffin wax transfers phase from solid to liquid or liquid to solid at a temperature nearly 26°C. In organic PCMs especially paraffin wax PCM, seems to be one of the more convenient latent heat storage materials able to used in building envelopes like mortar and concrete directly [6].

There are various techniques identified for the proper incorporation of PCM in building envelope material like, (a) Direct incorporation (b) Immersion (c) Shape stabilized (d) Encapsulation. Out of the above

IIOAB JOURNAL
ISSN: 0976-3104

mentioned techniques of PCM integration, encapsulation method having massive strength, durability, good thermal stability and avoids leakage/loss of PCM during phase transformation. Thermal energy storage combined with PCM is an smart idea for improving the thermal efficiency of the buildings. PCM can be integrated in the building envelope in various ways. One of the easiest and smart methods of integrating PCM directly in building envelope material is macroen capsulation. Due to this technique improve the indoor thermal comfort behavior of the buildings, but also reduces the cooling load without or little compromising with the mechanical strength of the building structure [7].

Microencapsulated Phase Change Material (MPCM) based thermal energy storage method has the substantially control the energy consumption of the buildings, by improving the indoor thermal comfort, when incorporated directly with the building envelope materials like cement, mortar, brick, wallboard, and gypsum successfully [8].

PCM plastering mortar, concrete, brick and cubicle construction materials with integrated PCMs are meant to promotes heat saving capacity, enable stabilization of indoor thermal of buildings whereby providing the thermal comfort condition also provides stability of indoor ambient temperatures. The thermal energy saving into the walls by encapsulating PCMs relatively with conventional concrete without PCMs promoted to an improved thermal comfortless as well as lower inner temperatures [5].

In this study going to investigate PCM encapsulated red-mud, geo polymer composites, under strength properties and binding between materials for PCM mortar possibility of usage in building materials. The phase change material is paraffin wax encapsulated with graphite powder used for preparing mortar. The mechanical strength and binding performance of red mud based PCM mortar is investigated under different mix proportions.

MATERIALS AND METHODS

Red-mud, quartz sand and sodium silicate/sodium hydroxide mixture was used to produce a red-mud based PCM mortar. The phase change materials concerns paraffin wax and graphite powder were used.

Various approaches have been applied for the integration of PCM to prepare mortar; whatever, direct mixing and replacement methods are normally used. The direct mixing techniques involves the PCM capsules additional composition in the Geo-polymer composite mortar, while the replacement techniques using the PCM capsules as a substitute to displace some percentage of sand within the Geo-polymer composite mortar [9].

Planning of PCM was most important step to make red mud based Geo-polymer PCM mortar. To accomplish the ideal characteristic of PCM cases first we played out a preliminary study to get familiar with the strategy engaged with planning of PCM. Utilizing 50 grams of graphite powder and same mass of paraffin wax was taken so as to get ready PCM mix. To facilitate the mixing of graphite powder and paraffin wax, the paraffin wax was melted to fluid stage at a temperature of 100°C (as appeared in Fig. 1) and afterward infused with the graphite powder for 1h in another to allow enormous as passage of the liquid paraffin into the graphite's voids. The subsequent stage was followed cautiously that was pouring dissolved wax on graphite capacity to make it a small capsule and afterward that small capsules was changed over in little containers (as appeared in [Fig.1]). The paraffin do used expandable graphite capsules was plunged into a mix of alkali solution so as to frame a surface protection and dried an ambient temperature by the paraffin for 24 h period. To prevent the cases of PCM from getting damage or breaking because of interior pressure, these cases were plunged into a Sodium hydroxide arrangement. Sodium hydroxide is a profoundly flexible substance and it acts a defensive coat to the microencapsulated PCMs.

Table 1: Mix Proportions of Red mud based PCM mortar

Raw Materials	Mix 1 (M1)	Mix 2 (M2)
Red Mud : Quartz Sand	15:85	25:75
PCM : RM & QS Mix	10:90	20:80

Red-mud and quartz sand and were thoroughly mixed physically for 10 min to permit total mix of the mixture to guarantee homogeneity; the effectively arranged alkali solution was added the homogenous blend and mixed ceaselessly for another 5 min. Subsequently the graphite powder PCM capsules were added into the red mud and quartz sand mix and mixed for other 5 min to finish the mixing procedure and at the mean time need prevent any damage to the PCM capsules. Distinctive various mix proportions have been utilized for the testing strength properties of PCM to plan testing strength in solid cubes. Mix proportions mentioned in [Table 1]. Three sample solid test cubes were made for each mix ratios under oven curing and normal curing methods. The cube size 70mm×70mm×70 mm is used. In the PCM mortar filled into the solid cubes that are remolded after 24hrs the kept the cubes in hot air oven at the temperature 41°C for 48hrs for curing rest of the sample solid cubes are kept in ambient temperature for normal curing process [11]. Table depicts the material various mix proportions used to set up the red mud based PCM incorporated geo-polymer mortar.

Fig. 1: PCM Preparation paraffin wax and graphite powder

Fig. 2: Mixing, Casting and Oven Curing

RESULTS

The PCM encapsulated red-mud geo polymer composite mortar was tested using the uniaxial compressive strength. Two test samples hot oven and normal curing is utilized for the strength test. The normal cured sample cubes are specimens that were provided to natural cooling, for hot oven curing temperature of 41°C till two days then subjected into normal ambient temperature before testing. The encapsulated PCM inside the red mud geo polymer composite was in solid and a liquid state for the cold cured and hot cured respectively. Mechanical strength test of the PCM red mud geo polymer mortar was conducted at different days (7, 14 and 28) respectively. The Indian standard code (IS 650, IS 4031) was followed for the compressive test; the test was conducted in triplicate. The average of each measured experimental samples tested was recorded [10].

Compressive strength is the point of captivity of a material to withstand loads liable to diminish size, instead of versatility, which withstands loads tending to extend. Compressive strength of strong cubes test results gives an idea in regards to all of the properties of concrete diverse standard codes supports reference or strong cube as the standard model for the test. Strength of the cubes determined following by after 7 days, 14 days and 28 days for both normal and hot air oven dried samples. Compressive strength recipe for any substance is the mass loaded at the motive of inability at the cross-section territory of the surface on which load was applied [13].

Compressive Strength = Load / Cross-sectional Area

Compressive strength is normally estimated by general UTM machine. The range from little table-top arrangements to ones with in excess of 50 MN limit. Determination of compressive strength is caused on the particular evaluate procedure and states of estimation. Compressive strength is typically detailed in relationship to a particular specialized standard. A total compressive strength of a substance is that determination of uniaxial compression load applied at when the sample gets failure fully. The compressive strength is ordinarily procured probably by strategies for a strength test [15].

Table 2: Compressive strength results

Compressive Strength	7 days (in N/mm2)	14 days (in N/mm2)	28 days (in N/mm2)
A. Normal curing sample- M1	2.3	5.28	7.75
B. Oven dried sample- M1	2.34	4.93	7.63
C. Normal curing sample- M2	1.4	4.25	6.34
D. Oven dried sample- M2	1.7	4.57	6.93

The red mud based PCM encapsulated geo polymer mortar was evaluated under two different curing methods and loading conditions, inside the matrix. [Table 2] shows the average compressive strength of 2 samples these being the hot oven and normal curing sample cubes treated red mud PCM mortar surfaces respectively. Estimation of the compressive strength for sample specimens in [Table 2] showed variations in the process parameters, consisting to mechanical behavior. The compressive strength was found to increase as the curing days prolonged in both hot oven and normal curing cases [9].

IIOAB JOURNAL
ISSN: 0976-3104

Specimen sample A and B had the highest compressive strength with 7.7 and 7.6 N/mm2 for hot oven and normal curing conditions, respectively. The quantity of PCM in the mortar design matrix was also identified to impacts in the comprehensive strength. A 31% comprehensive strength improvement was observed from day 14 days to 28 days both curing samples, In according with the shift in the compressive strength with respect to quantity fraction of the incorporated PCM into geo polymer mortar was observed on both cases. The curing duration influences on mechanical strength properties of the PCM composites: the enlarged the curing duration for both curing methods, increasing and decreasing comprehensive strengths. The pore structure appears to be enhanced because porosity decreased, thereby enhancing the expandable graphite strength because of the introduced encapsulated PCM within the geo polymer matrix. The compressive strength of the red mud based PCM mortar was mostly depended by the curing duration and the amount of PCM concentration within the design matrix. The output of strength implies, more than half of the final red mud based PCM mortar strength is improved nearly the last 28 days. This outcome is in accordance with other observations in literature is not acceptable. The difference in comprehensive strength between the hot oven and normal curing cases can be possessed to the curing temperature influence on the PCM geo polymer mortar, nevertheless no significant effects was identified for the comprehensive strength properties of the PCM geo polymer mortar at prolonged heating. Thus, it can be conclude that the phase changes from solid to liquid and liquid to solid of the PCM was not influenced in the matrix mortar.

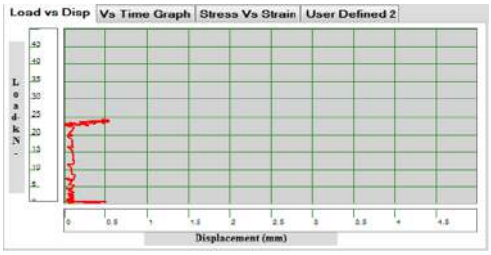

Fig. 3: Load vs. Displacement graph (14 days Oven dried cube).

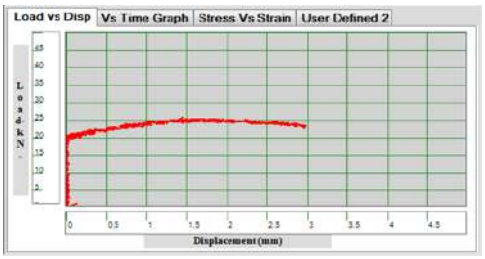

Fig. 4: Load vs. Displacement (14 days normal curing).

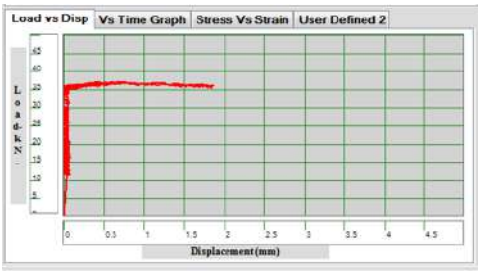

Fig. 5: Load vs. Displacement (28 days normal curing).

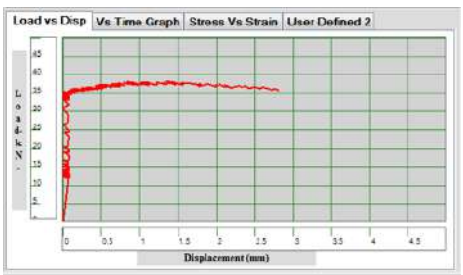

Fig. 6: Displacement vs. Time (28 days Oven dried cube).

IIOAB JOURNAL
ISSN: 0976-3104

DISCUSSION

Direct mixing method it needs to confirm first the encapsulated PCM within a chemically and physically stable condition. This is essential to maintain the PCM in its original form and ensure no incorporation with the construction envelope materials [10].

According to this study the possibility using phase change materials for preparing red mud based PCM mortar with direct mixing method. In this concerns focused to identify the strength and bonding properties of red mud based PCM mortar was investigated for the further investigation of thermal energy managing in buildings. Based on the results of this study represents there is no issues according to the bonding behaviors in between red mud and PCM materials on different mix proportions, at the mean time to need to achieve the better binding capacity is needed for red mud based PCM mortar may make it possible to use in construction and building applications. Red mud based PCM mortar also has some undesirable properties such as lower strength comparatively standard mortar values mentioning in Indian standard codes. These undesirable properties of this PCM mortar leads unable to suggest directly applicable for building materials without evaluated from further studies, however, can be possible if appropriate PCM types and means of incorporation with better conventional materials are employed.

CONCLUSION

Another approach was successfully developed for improved building envelope materials, using PCM as paraffin wax encapsulated with graphite powder with other additives of quartz sand, red-mud and alkaline activator mixtures. The impacts of red-mud based PCM mortar with respect to the compressive strength and bonding properties was determined in this study finally the following points are highlighted from the experimental results.

1. The different in structural properties with two design matrix of red mud and quartz sand was investigated to achieve the optimum ratio incorporated with PCM from these Mix 1 represents better with other matrix.
2. Binding Property of red mud based PCM mortar as useful for both normal curing and oven dried curing red mud based PCM mortar samples. The amount of encapsulated PCM incorporation in different matrix does not affect the bonding behaviors of mortar.
3. Compressive strength of sample specimens tested following 7 days, 14 days and 28 days for both normal curing and oven dried curing red mud based PCM mortar. In view of the compressive strength outcome 28 days result was seen to be better to 14 days test result comparatively Mix 1 shows better results. Yet, the mechanical strength was not satisfied comparing standard values recommended by Indian standard codes respecting with conventional mortar already using in field.
4. To satisfy the standard recommendations for mortar, just red mud isn't sufficient for strength and furthermore there is should be another kind of binding material and another possible technique is needed for improving and achieving the better strength characteristics of red mud based PCM mortar.
5. A further investigation is required to accomplish better outcomes concerning the change for conventional materials for achieving sustainable building sector.

CONFLICT OF INTEREST

The authors declare no conflict of interest relating to the material presented in this paper.

ACKNOWLEDGEMENTS

The corresponding author would like to thank the Manav Rachna International Institute of Research and Studies for providing the platform for conducting the research. This support was gratefully acknowledged.

FINANCIAL DISCLOSURE

None.

REFERENCES

[1] Bano F, Sehgal V. [2018] Evaluation of energy-efficient design strategies: Comparison of the thermal performance of energy-efficient office buildings in composite climate, India. Solar Energy, 176:506–519.
[2] Beltran RD, Martinez-Gomez J. [2019] Analysis of phase change materials (PCM) for building wallboards based on the effect of environment. Journal of Building Engineering, DOI: 10.1016/j.jobe.2019.02.018.
[3] Frazzica A, Brancato V. [2019] Thermal performance of hybrid cement mortar-PCMs for warm climates application. Solar Energy Materials and Solar Cells, 193:270–280.
[4] Lukmon AO, Ariff ZM. [2019] Red-mud geo-polymer composite encapsulated phase change material for thermal comfort in built-sector. Solar Energy, 181:464–474.
[5] Mankel C, Caggiano, A. [2019] Thermal energy storage characterization of cement-based systems containing microencapsulated-PCMs. Construction and Building Materials, 199:307–320.
[6] Rao VV, Parameshwaran. [2017] PCM-mortar based construction materials for energy efficient buildings: A review on research trends. Energy and Buildings, https://doi.org/10.1016/j.enbuild.2017.09.098.

[7] Rathore, PK, Shukla SK. [2019] An Experimental Evaluation Of Thermal Behavior Of The Building Envelope Using Macro encapsulated PCM For Energy Savings. Renewable Energy, https://doi.org/10.1016/j.renene.2019.10.130.
[8] Rathore, PK, Shukla SK. [2019] Potential of macro encapsulated pcm for thermal energy storage in buildings: A comprehensive review. Construction and Building Materials, 225:723–744.
[9] Ricklefs A, Thiele AM. [2017] Thermal conductivity of cementitious composites containing microencapsulated phase change materials. International Journal of Heat and Mass Transfer, 104:71–82.
[10] Saxena R, Rakshit D. [2019] Phase change material (PCM) incorporated bricks for energy conservation in composite climate: A sustainable building solution. Solar Energy, 183:276–284.
[11] Standard I. [2005] IS 4031, Part-6 Methods of physical tests for hydraulic cement. India.
[12] Standard I. [2008] IS 650 Standard sand for testing cement specification.
[13] Shetty MS. [2005] Concrete technology. S Chand & company LTD.420-453
[14] Neville AM, Brooks JJ. [1987] Concrete technology England: Longman Scientific & Technical, 242-246.
[15] Gambhir ML. [2013] Concrete technology: theory and practice. Tata McGraw-Hill Education.

ISSN: 0976-3104
ISSUE: Science and Technology

ARTICLE

FPGA BASED DESIGN AND ARCHITECTURE OF NETWORK-ON-CHIP ROUTER FOR EFFICIENT DATA PROPAGATION

Hirebasur Krishnappa Krutthika*, Anur Rangappa Aswatha

Department of Electronics and Communication Engineering, Dayananda Sagar College of Engineering, Bengaluru-560 078, Karnataka, INDIA

ABSTRACT

Network on Chip (NoC) architectures are proposed to address the communication problems and various fabrication issues in block-based design existing in System on Chip (SoC). In this paper, an efficient NoC router architecture is proposed to route the data from one block to other structurally. For proper routing operation, the proposed architecture has bidirectional data transfer capabilities with design of an efficient controller to control and synchronize the overall operations. The FIFO is optimized for efficient handling of the data, which are transferred in different directions. To generate optimized hardware architecture, various optimization techniques are used at the architectural level. As a result, the overall performance of the architecture is improved than the existing architectures which further proved in the comparison table.

KEY WORDS
System on Chip, Network on Chip, FPGA Architecture, Router, XY Routing, FPGA.

Received: 7 Oct 2020
Accepted: 18 Dec 2020
Published: 19 Dec 2020

***Corresponding Author**
Email:
krutthika-ece@dayanandasagar.edu
Tel.: 91- 9886421452

INTRODUCTION

Network on Chip (NoC) architectures are commonly used in designing of high-speed integrator circuit architectures [1] that provides various advantages over commonly used for data transfer technique. Basically, a sophisticated controller is used to control the data flow, but in many real time circumstances, due to various fabrication issues, the problem arises with the controller. Also, many of the sophisticated controllers used dedicated path for data transfer which was decided before the data transmission and this fails to achieve optimized results whenever the traffic flow in that path was high. So there is a need for intelligence for the circuit to decide at real time to decide the exact path of data transfer. This situation can be overcome by using NoC, instead of a sophisticated controller where each module can take own decision of transferring the data depending upon the routing logic. This achieves better speed for the transfer of data and also it can be able to send the data through some other alternative path. The existing NoC hardware architectures have many limitations with effective handling of buffers for data transfer, hardware implementation and synchronization issues. In this paper, we have proposed an efficient VLSI architecture to implement a NoC where we have addressed the buffering issues.

Various types of NoC architectures are proposed for efficient implementation. Among these implementations some of works are as follows: In paper [2] the authors have proposed an architecture in which the Memory Management Unit (MMU) is implanted in Network-on-chip (NoC) and therefore the MMU functionality in the proposed NoC was implemented without any modifications in the processor design. It also supports for multiprocessing required for the dedicated high-speed processing applications. The proposed architecture consumed 16~23% more resources requirements. In paper [3] the authors have proposed Open NoC (Open-Source Light Weight deflection torus-based NoC) with PCIe-based communication controller. This method saved the event time and also has the higher clock performance. This also was adapted in many other high-speed communication technologies to operate at higher speed. The trade-off lies with disadvantage of more LUT are compared to Hoplite with respect to the implementation for AXI4 stream interface. In [4] the authors have proposed the design of NoC RingNet using FPGA. In this method, the architecture has consumed a smaller number of resources in terms of LUT's and Flip-flops. This method supported higher clock frequencies with portability for many applications. The distributed RAM available in FPGA's are used to implement buffers and an efficient virtual cut-through switching technique used to reduce latency. The FPGA based Multi-accelerators and Chip-Multiprocessor (CMPs) connected through the NoC is proposed in [5]. This proposed method is light-weight and scalable in characteristics. The proposed method has the high performance in terms of latency and throughput. The NoC simulator, titled Dual-Clock router micro-architecture (DuC-NoC) is elaborated in paper [6]. Furthermore, the authors have implemented two-layer configurable global interconnection to minimize the time overhead, to make an efficient trade-off between simulation time of the entire simulator and also the resource utilization. The advantage of this approach is that, it can simulate 2048 nodes virtualized Mesh Network. In paper [7] the authors have proposed the CDMA spreading codes which further increased to emphasize the capacity of CDMA Network-on-Chip (NoC) crossbars. The simulation results in the paper showed the sharp increase in the bandwidth utilization with a lesser amount of resource utilization and by reducing the facility consumption by 45. The proposed NoC based network architecture in [8] has modified router architecture which is optimized at architectural level. The integrated run-time solution for security and fault tolerance FPGA based System on Chip through digital signatures supported by x-network is proposed in [9]. By implementing the digital signature technique, the numbers of routers used for designing a network are reduced and also offer more flexibility. The network design has used 10% more LUT's compared to traditional methods for both security and fault tolerant features. In paper [10], the authors have proposed butterfly-based NoC's and ASIP (Application Specific Instruction Set Processor) architecture. The benefits of this method are, it supports modulation schemes from BPSK to 256-QAM for

any mapping style and eight stages single & double binary codes. The disadvantage is that, extra hardware cost is required to enable turbo demodulation.

Contributions: The main contributions of this research paper are,

- Design of an efficient controller to control and synchronize the overall operations in NoC.
- The existing FIFO architecture is modified to get proper status signal for the data buffering and also the FIFO is implemented using lesser hardware requirements.

This research paper is organized as follows, In Section 1, the methodology of the proposed architecture and its internal block diagrams are explained in detail, followed by Section 2, the implementation on FPGA and results are discussed and the lastly comparisons with existing techniques are given in Section 3.

MATERIALS AND METHODS

The proposed enhanced NoC architecture is shown in [Fig. 1]. The modules in the architecture consist of Concatenation module which formats the data as per the requirement, Controller module to control and synchronize all the operations and lastly the modified Memory blocks which stores the intermediate data. The data can be accepted from any direction and can be routed to any other direction using proposed an adaptive routing algorithm. The proposed architecture has four input and output ports in respective directions, which can be categorized as East, West, North and South. To perform proper routing operation, the data format should in the appropriate format, where the source and destination addresses is surrounded within the data. The main function of the concatenation block is to extract only the data. After the data extraction process, the source and destination addresses are analyzed to route the data to the specific port. In some specific cases, the data is stored temporarily by the modified memory unit.

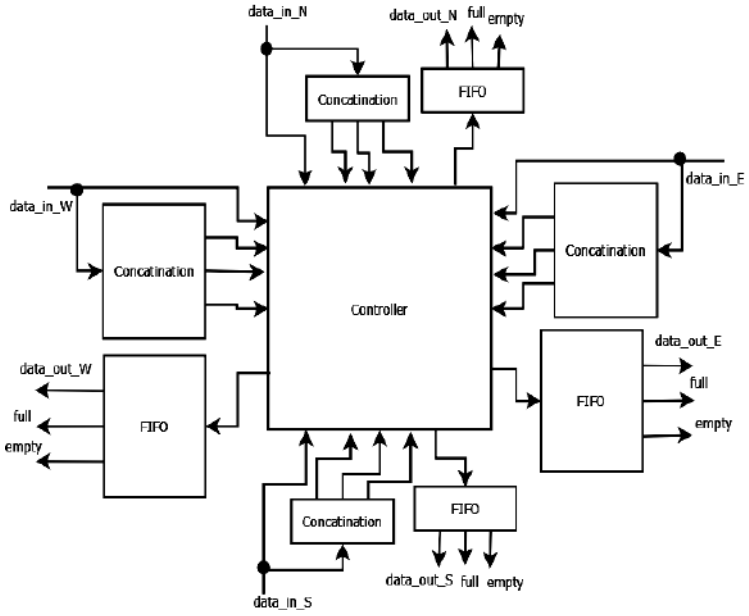

Fig. 1: The Proposed NoC Architecture

Data format

For proper routing purpose, it is essential for any routing algorithm to get the destination address of the data packet. As a result, the data format is used to implement the proposed architecture is shown in [Fig. 2]. In this case, the data is of 8 bits and the total address is of 4 bits where each field (i.e., X and Y) addresses consisting of 2-bits each. As and when the data packet arrives, the addresses are extracted and processed based on the X and Y addresses and the data will be delivered to appropriate port using the X-Y routing algorithm.

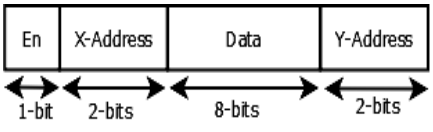

Fig. 2: Data Format

Concatenation

The extraction of destination address is done by concatenation block. The concatenation block is shown in [Fig. 3], which comprises of the Concatenation-1, Concatenation-2 and Concatenation-3 blocks respectively.

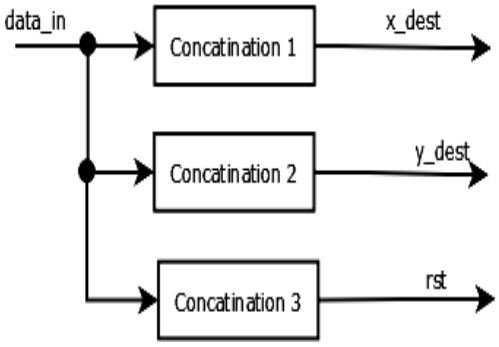

Fig. 3: Concatenation architecture

The Concatenation-1 and Concatenation-2 blocks are used to generate 'X' and 'Y' address of the destination router. The pseudo code is used to design Concatenation-1 is given in Pseudo code 1.

Pseudocode 1:

```
if (rst=0)
{
data_out =0
}
else if (Positive Edge clk)
{
X_dest=data_in (11 downto 10)
 }
end if
```

Similarly, the pseudocode for Concatenation-2 block is given in Pseudocode 2. Finally, the Concatenation-3 block is used to extract the 'rst' field data, which is used by the module as 'req' signal which acts as request signal to the appropriate router for establishing exact routing path. The pseudocode which is used to build this block is given in Pseudocode 3.

Pseudocode 2:

```
if (rst=0)
{
data_out =0
 }
else if(Positive Edge clk)
{
rst_dest=data_in (12)
}
end if
```

Pseudocode 3:

```
if(rst=0)
{
data_out =0

}
else if(Positive Edge clk)
{
Y_dest=data_in (1 downto 0)
 }
end if
```

Controller

The controller basically controls the data path for proper routing of data. It consists of MUX, DEMUX, D Flip Flop and modified X-Y routing algorithm respectively. The controller block is shown in [Fig. 4].

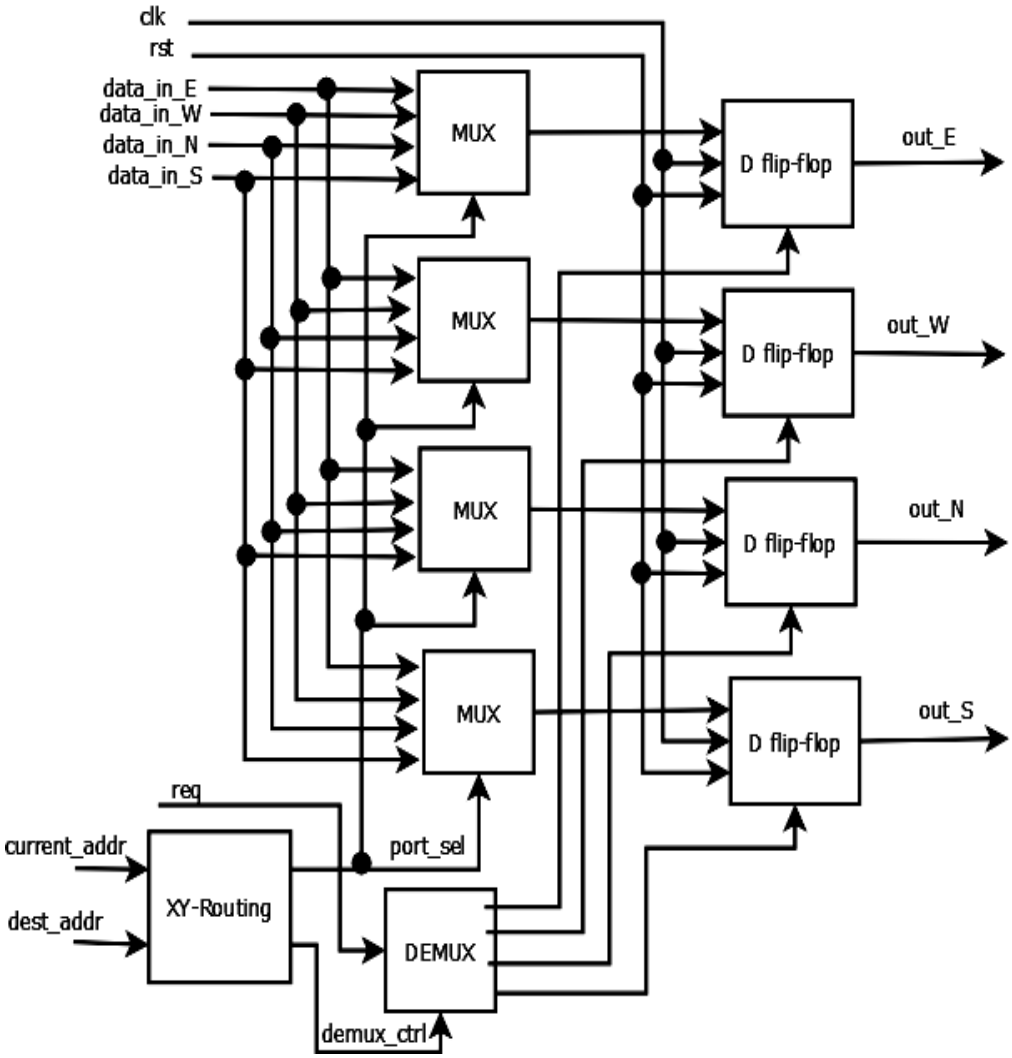

Fig. 4: Hardware architecture of proposed Controller

The controller block decides the proper routing path using modified X-Y routing algorithm. It generates the control signal for controlling the MUX and DEMUX blocks. For this purpose, the modified X-Y routing algorithm generates a "port-sel" and "demux-ctrl" signals where, the "port-en" signal is used to route the proper input data through "MUX" block and the "demux_ctrl" signal is used to route the request signal through "DEMUX" block, which act as reset switch for D-flip flops respectively. The output of the MUX and DEMUX blocks are connected to the respective D-flip flops for establishing proper routing path. The MUX and flip flops are properly synchronized with clock so that, the data mismatch does not occur.

X-Y Routing algorithm

The traditional routing algorithm used is the basic X-Y routing algorithm, [11] presented the data transmission between the cores. The main advantage of this algorithm is, it is to implement in hardware and also gives good trade-off between different parameters. The flowchart of the X-Y routing is given in [Fig. 5].

FIFO

The FIFO's are used to store data briefly. In this case, here it is used to synchronize the data temporarily, when the next router is busy in accepting the data packet. The architecture of modified FIFO is shown in [Fig. 6], which consists of FIFO and the indicator block where it is used to indicate the state of the FIFO (i.e., full or empty).

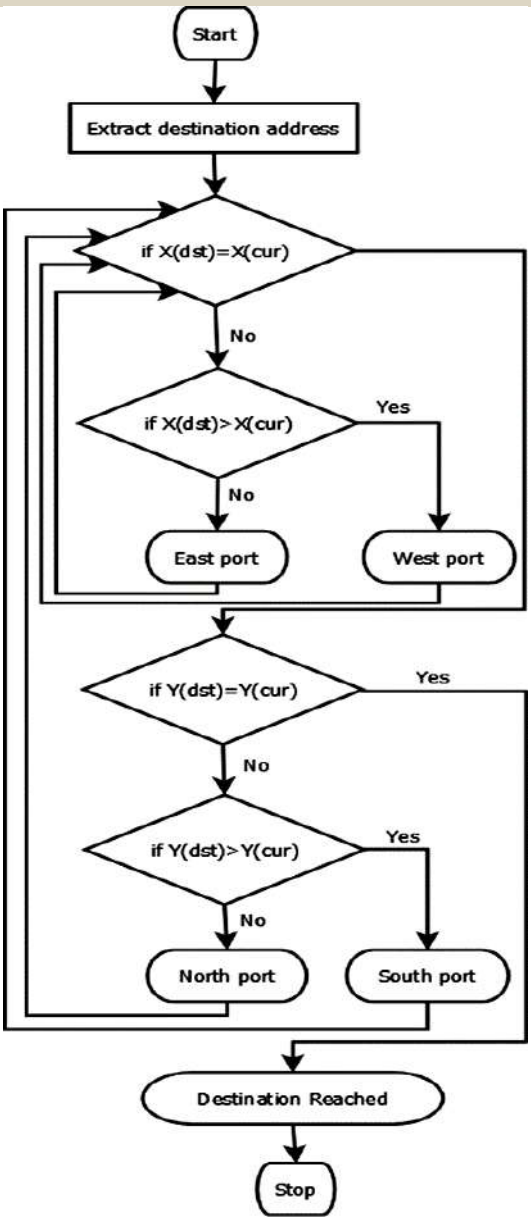

Fig. 5: X-Y Routing Algorithm

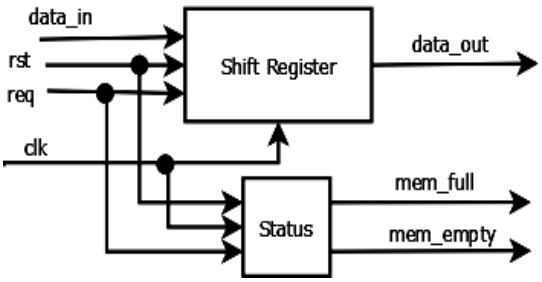

Fig. 6: Hardware architecture of modified FIFO

To optimize the indicator block, the Finite State Machine (FSM) module is implemented. The proposed FSM model implementation is done through Pseudo code 4.

Pseudocode 4:

```
if (rst=0 & (req=1 or req=0))
{
```

```
pointer=0
mem_empty=0
mem_full=0
 }
else
      {
if(positive edge clk)
      {
if(pointer<N)
      {
pointer=pointer+1
mem_empty=1
mem_full=0
      }
else
     {
pointer=pointer
mem_empty=0
mem_full=1
}
end if
}
end if
end if
```

RESULTS AND DISCUSSION

FPGA implementation

The proposed architecture is implemented in Digilent Atlys FPGA [12, 13] board through Xilinx ISE tool [14] and the coding is done using VHDL language [15]. The hardware utilization of the proposed NoC architecture with the sub modules are given in [Table 1].

Table 1: Hardware utilizations of proposed architecture

Parameters	Concatenation	XY-Routing	FIFO	Values
FPGA	Spartan-6 (XC6SLX45-3CSG324)			
Slice Registers	0	0	17	122
Slice LUTs	2	20	23	141
LUT-FF Pairs	1	11	17	103
Maximum Frequency (MHz)	-	-	297.987	373.413

The RTL schematic gives the gate level connection, the illustration of the enhanced design in terms of generic symbols, such as adders, multipliers, counters, AND gates, and OR gates, is generated by the Xilinx tool is shown in [Fig.7].

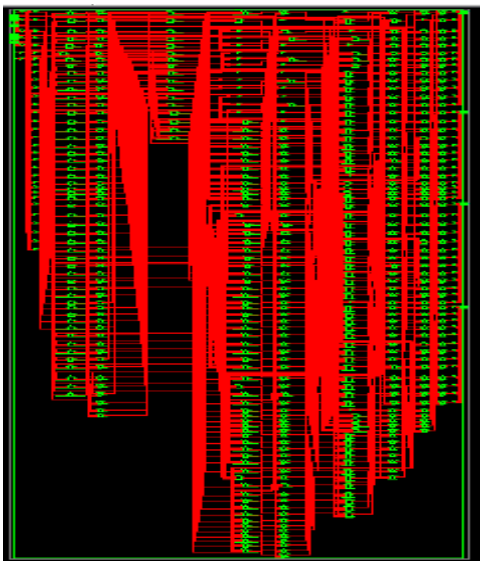

Fig. 7: RTL schematic of the proposed NoC architecture

Similarly, the generated technology schematic is shown in [Fig. 8] such as LUTs (Look Up Tables), Carry logic and I/O buffers and other components are shown.

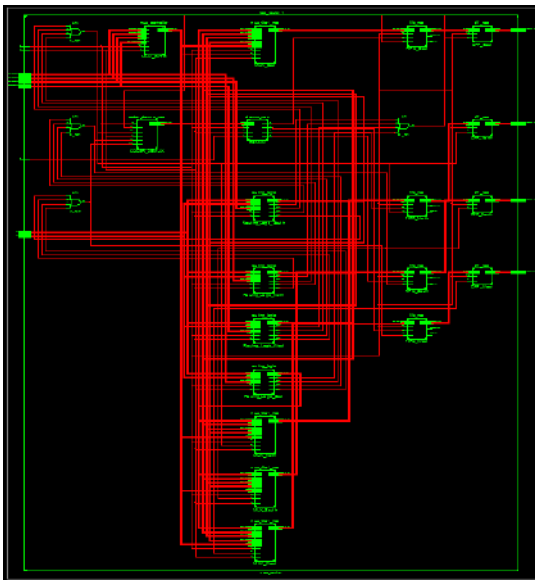

Fig. 8: Technology schematic of the proposed NoC architecture

Simulation

The timing diagram of proposed NoC router is shown in the [Fig. 9] where timing of each tasks are shown which takes one clock cycle.

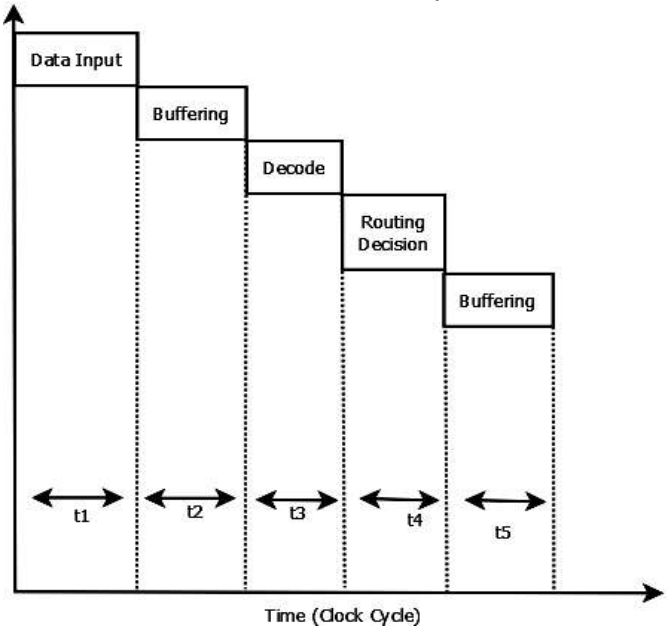

Fig. 9: Timing diagram of the proposed NoC

The simulation results of the proposed NoC router is shown in the [Fig. 10] to [Fig. 13] for different cases given below.

Case 1

The simulation result of NoC router in [Fig. 10] transfers the data at West port through proper destination address.

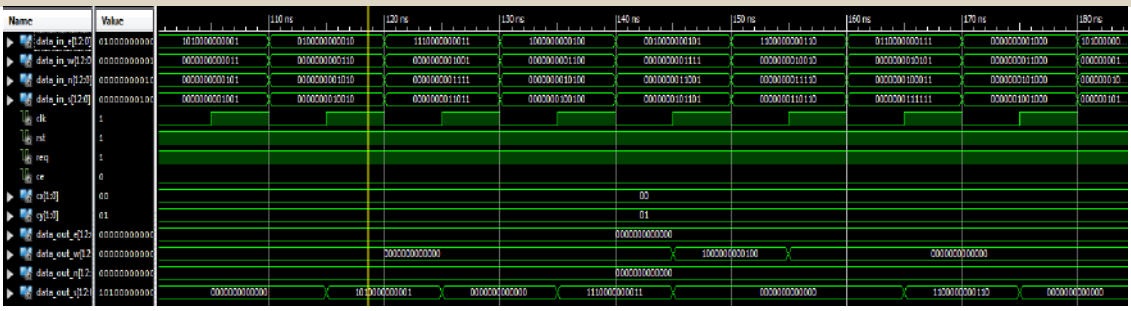

Fig. 10: Simulation result of the proposed NoC transferring data at West Port

Case 2

The simulation result of NoC router in [Fig. 11] transfers the data at East port through proper destination address.

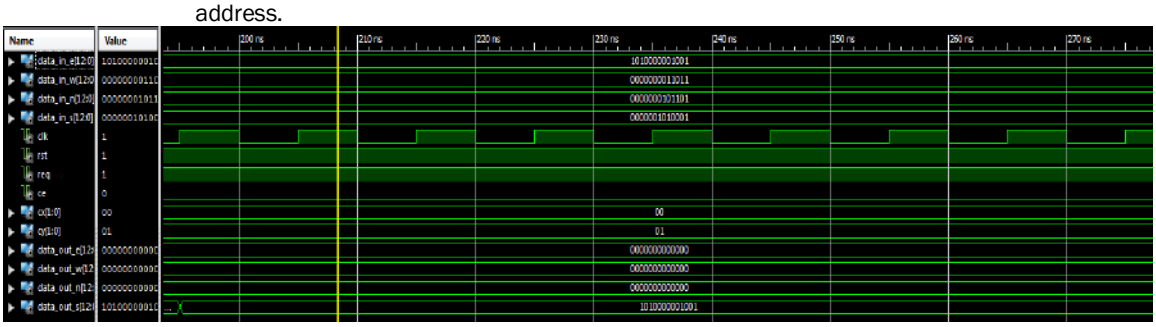

Fig. 11: Simulation result of the proposed NoC transferring data at East Port

Case 3

The simulation result of NoC router in [Fig. 12] transfers the data at North port through proper destination address.

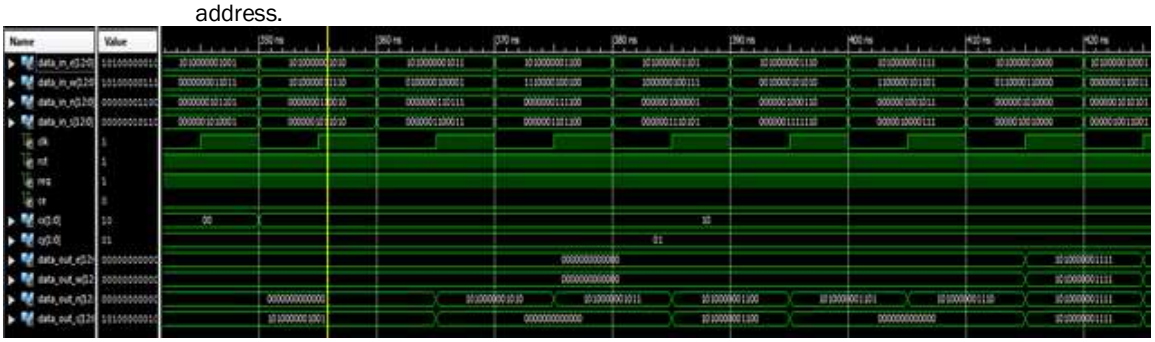

Fig. 12: Simulation result of the proposed NoC transferring data at North Port.

Case 4

The simulation result of NoC router in [Fig. 13] transfers the data at East port through proper destination address.

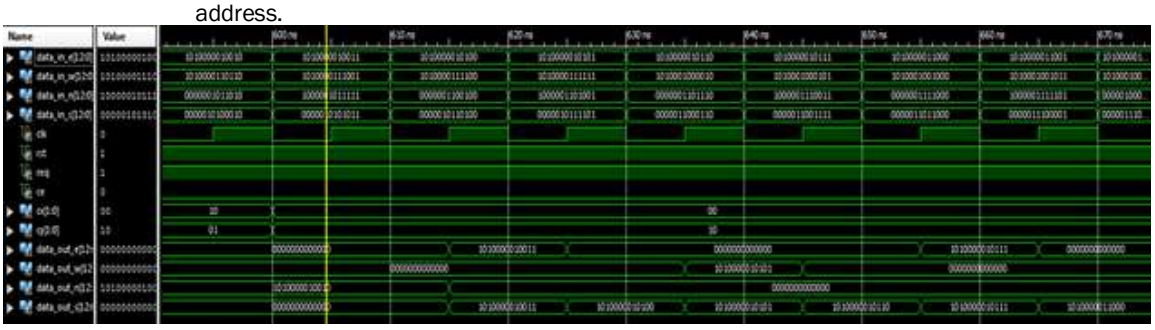

Fig. 13: Simulation result of the proposed NoC transferring data at South Port.

The comparison of the proposed NoC architecture with the existing NoC architectures are compared with respect to the hardware parameters is shown in [Table 2]. In [16] the authors have proposed the FSM based model. Here, with the growth in the number of redundant nodes, the overall hardware utilization in the architecture increases. This intern has increased the Look Up Table (LUT)- Flip Flop (FF) pairs and also the operating frequency. The increase in the LUT-FF pairs occupies more area and power. Similarly, in paper [17] the authors have presented the architecture which uses, large area due to the use of un-optimized FIFO architecture. Here also, when compared to paper [16], the LUT-FF pairs have been reduced minimally. But when compared to our proposed NoC architecture, both these parameters are addressed effectively to achieve optimization with respect to the area and throughput.

Table 2: Comparison table of the existing and proposed NoC architectures

Parameters	Raaed Faleh, et al. [16]	Santrupti M, et al. [17]	Proposed Architecture
FPGA	Spartan-3A	Spartan-6	Spartan-6
Slice Registers	-	224	122
Slice LUTs	-	162	141
LUT-FF Pairs	1861	128	103
Maximum frequency (MHz)	82.734	292.987	373.413

CONCLUSION

The proposed hardware architecture performs the routing of the data efficiently using NoC methodology which performs; various optimization techniques using FSM modelling are realized. The optimized NoC architecture is compared with other existing architectures to validate the result and there is a significant increase with respect to the area and throughput are realized. The future work includes the design and techniques used for 2D NoC architectures can be upgraded to 3D NoC architectures as the layout and algorithms used for data propagation is unique and complex. Our main goal for 3D NoC is to concentrate on the performance parameters of NoC architectures.

CONFLICT OF INTEREST

There is no conflict of interest.

ACKNOWLEDGEMENTS

This work was carried out in the Department of Electronics and Telecommunication Engineering department, Dayananda Sagar College of Engineering Bengaluru.

FINANCIAL DISCLOSURE

None.

REFERENCES

[1] Hyeonguk J, Kyuseung H, et al. [2019] MMNoC: Embedding Memory Management Units into Network-on-Chip for Lightweight Embedded Systems, IEEE Access, 4: 80011 – 80019.

[2] Reddy KS, Vipin K. [2019] OpenNoC: An Open-Source NoC Infrastructure for FPGA-Based Hardware Acceleration. IEEE Embedded Systems Letters, India, 11(4): 123 – 126.

[3] Jakub S, Adam Ł, et al. [2019] Ring Net: A Memory-Oriented Network-On-Chip Designed for FPGA. IEEE Transactions on Very Large-Scale Integration (VLSI) Systems, 27(6):1284 – 1297.

[4] Lin Z, Sinha S, et al. [2018] Scalable Light-Weight Integration of FPGA Based Accelerators with Chip Multi-Processors, IEEE Transactions on Multi-Scale Computing Systems, 4(2): 152 – 162.

[5] Hadi MK, Kimia Z A, et al. [2018] DuCNoC: A High-Throughput FPGA-Based NoC Simulator Using Dual-Clock Lightweight Router Micro-Architecture, IEEE Transactions on Computers. 67(2): 208 – 221.

[6] Ahmed KE, Mohamed R, et al. [2017] Overloaded CDMA Crossbar for Network-On-Chip, IEEE Transactions on Very Large-Scale Integration (VLSI) Systems, 25(6):1842 – 1855.

[7] Abdelfattah SM, Bitar A, et al. [2017] Design and Applications for Embedded Networks-on-Chip on FPGAs, IEEE Transaction on Computers. 66(6): 1008 – 1021.

[8] Vijayalaxmi J, Satish B. [2018] An Efficient FPGA Based NoC Architecture for Data Communication, International Journal of Advanced Computer Research, 8(39):335-341.

[9] Raza AJ, Amer B, et al. [2017] Heterogeneous Multi-ASIP and NoC-Based Architecture for Adaptive Parallel TBICM-ID-SSD, IEEE Transaction on Circuits and Systems. 65(3): 259 – 263.

[10] Yao C, Swathi T, Gurumani, et al. [2016] FCUDA-NoC: A Scalable and Efficient Network-on-Chip Implementation for the CUDA-to-FPGA Flow IEEE Transactions on Very Large-Scale Integration (VLSI) Systems, 24(6): 2220 - 2233

[11] Priti S, Narayan P. [2019] Modified X–Y routing for mesh topology based NoC router on field programmable gate array, IET Circuits Devices & Systems, Devices and Systems. 13(3): 391.– 398.

[12] https://reference.digilentinc.com/reference/programmable-logic/atlys/start. (Accessed on 15 May, 2020)

[13] Satish B, Sayantam S, et al. [2018] FPGA Implementation of Optimized Karhunen–Loeve Transform for Image Processing Applications. Journal of Real-Time Image Processing, 17(6):357–370.

[14] https://www.xilinx.com/support/documentation/sw_manuals/xilinx14_1/ise_tutorial_ug695.pdf (Accessed on 18 May, 2020)

[15] Roth CH [1997] Digital Systems Design Using VHDL, PWS Publishing Company, Boston, MA, USA

[16] Raaed F, Raaed H, et al. [2018] Hardware Implementation of NoC based MP-SoC Prototype using FPGA, International Journal of Applied Engineering Research, 13(7): 5443-5451.

[17] Santrupti SM, Sayantam S, et al. [2016] FPGA Implementation of High Speed and Low Area Four Port Network-On-Chip (NoC) Router, IOSR Journal of VLSI and Signal Processing (IOSR-JVSP), 6(6): 52-57.